GLOBAL AND LOCAL MODE-DOMAIN ADAPTIVE ALGORITHMS FOR SPATIAL ACTIVE NOISE CONTROL USING HIGHER-ORDER SOURCES

Naoki Murata[⋆] *Jihui Zhang*[†,*] *Yu Maeno*[⋆] *Yuki Mitsufuji*[⋆]

[⋆] Sony Corporation, Minato-ku, Tokyo, Japan
[†]Research School of Engineering, The Australian National University, Canberra ACT 2601, Australia

ABSTRACT

The aim of spatial active noise control (ANC) is to attenuate noise over a certain space. Although a large-scale system is required to achieve spatial ANC, mode-domain signal processing makes it possible to reduce the computational cost and improve the performance. A higher-order source (HOS) has an advantage in sound field control due to its controllable directivity patterns. An array of HOS can suppress an undesired exterior sound propagation while occupying a smaller physical space than a conventional omnidirectional loudspeaker array. In this paper, we propose two types of adaptive algorithm for spatial ANC using HOSs, which provide a trade-off between efficiency and error robustness against loudspeaker placements. Numerical simulations in a reverberant environment show the efficacy of the proposed algorithms compared with the conventional multipoint adaptive spatial ANC algorithm.

***Index Terms*—** Active noise control, adaptive algorithm, mode-domain signal processing, higher-order sources, filtered-X LMS

1. INTRODUCTION

Active noise control (ANC), or noise cancellation, aims to attenuate primary (unwanted) noise by generating anti-noise from secondary sources. There are a number of applications of ANC, such as noise-cancelling headphones [1], ANC systems in automobiles [2], and ANC systems in ducts [3]. Since acoustic noise is usually unknown and varies with time, ANC systems employ an adaptive structure to cope with these variations. Most common adaptive methods employ the least-mean-squares (LMS) algorithm and its variants [4–6].

Spatial ANC, which aims to attenuate noise over a certain space, is a major research interest. Since not only one spatial point but a space has to be controlled, a number of transducers are required. A straightforward way to achieve spatial ANC is to extend the single-channel filtered-X LMS (FxLMS) algorithm to a multichannel setup [7]; however, this method has two drawbacks. First, only the sum of the squared pressures at microphone locations is considered to be reduced; there is no guarantee that the total amount of noise over the space is also reduced. Second, the computational cost of the multichannel ANC system rapidly increases with the number of transducers.

To overcome these problems, several methods based on mode-domain signal processing were proposed, by which the sound field is decomposed into orthogonal basis functions, e.g., the fundamental solutions of the Helmholtz wave equation [8]. The computational cost can be significantly reduced because mode-domain conversions reduce the cross-correlations between transducers and the filter update can be computed in a mode-independent manner [9–12]. Moreover, noise attenuation over the entire space of interest can be achieved by controlling the mode-domain coefficients over a region rather than the pressures at multiple locations [9–13].

* The work was done during Sony's summer internship program.

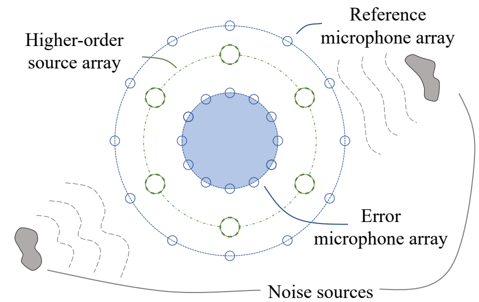

Fig. 1: Array configuration.

Despite the advantages of the mode-domain approach, there are still some difficulties in implementing a large-scale system. One of the major problems is that loudspeakers occupy more space than microphones because a large volume is required for enclosures to produce a sufficiently strong l ow-frequency signal. The acoustic feedback from loudspeakers to the reference microphones is also a problem that deteriorates the robustness of the system.

Higher-order sources (HOSs), a.k.a. higher-order loudspeakers, have been applied to spatial audio use-cases [14–20] and sound attenuation outside the loudspeaker array has been reported. An array of few condensed HOS can achieve the same performance as the large-scale conventional loudspeaker array. Additionally, the controllable directivity patterns of HOS can suppress the undesired acoustic feedback sound propagation from the secondary sources to the reference microphones.

In this paper, we propose two types of mode-domain adaptive algorithms exploiting HOSs, which provide a trade-off between efficiency and error robustness to loudspeaker placements. Both proposed algorithms minimize the LMS between the mode-domain signals, and thus can reduce the computational cost significantly compared with the method in [21]. Numerical simulations in a reverberant environment show the efficacy of the proposed algorithms, and the algorithms were compared.

2. PROBLEM FORMULATION

In this paper, we consider a two-dimensional (2D) sound field for simplicity. The proposed method can be extended to a three-dimensional (3D) case with some modifications.

2.1. Array configuration

Figure 1 shows the array configuration assumed in this paper. There are three concentric equiangular arrays: an error microphone array, an HOS array, and a reference microphone array. The numbers of transducers in the reference array, HOS array, and error array, and their indices are denoted as N_r, N_l, N_e, i_r, i_l, and i_e, respectively. The radii of the arrays are denoted as r_r, r_l, and r_e. The angles of the transducers are denoted as ϕ_{i_r}, ϕ_{i_l}, and ϕ_{i_e}. Our objective here is to attenuate noise in the area surrounded by the error microphone array (hereafter, called the target area).

2.2. Harmonic representation of sound field

Assuming that the target area is circular with the center at the origin and a radius of r_{target}, the sound field in this area is represented using the harmonic representation as [22]

$$p(k, \boldsymbol{r}) = \sum_{m_g=-M_g}^{M_g} J_{m_g}(kr)\gamma_{m_g}(k)e^{-jm_g\phi}, \tag{1}$$

where $\boldsymbol{r} = (r, \phi)$ is an arbitrary point in polar coordinates. $k = 2\pi f/c$ is the wave number, where f and c denote the time frequency and velocity of sound, respectively. $J_m(\cdot)$ denotes the Bessel function of order m. We name the order of the sound field representation as the global order and denote its index as m_g to distinguish it from the order of the HOS, which is defined later. The global mode coefficients are denoted as $\gamma_{m_g}(k)$ for the same reason. Hereafter, k is sometimes omitted for notational simplicity. Although the above summation should be summed up to infinite order, a maximum truncation order of the global mode coefficients is set in practice with some criteria, such as $M_g = \lceil kr_{\mathrm{target}} \rceil$ [23] or $\lceil kr_{\mathrm{target}} \rceil + 1$ [24], where $\lceil \cdot \rceil$ denotes the ceiling function.

The global mode coefficients of the sound field are calculated using the signals received by the microphone array. When the signals of the error microphone array $\boldsymbol{e} = [e_1, \cdots, e_{N_e}]^T \in \mathbb{C}^{N_e \times 1}$ are measured ($(\cdot)^T$ denotes the transpose operator of a vector), they are transformed into the global mode coefficients $\boldsymbol{\epsilon} = [\epsilon_{-M_g}, \cdots, \epsilon_{M_g}]^T \in \mathbb{C}^{(2M_g+1)\times 1}$ as [25]

$$\epsilon_{m_g} = \frac{1}{N_e J_{m_g}(kr_e)} \sum_{i_e} e_{i_e} e^{jm_g\phi_{i_e}}, \tag{2}$$

where $i_e = 1, \cdots, N_e$. Similarly, the global mode coefficients $\boldsymbol{\beta} \in \mathbb{C}^{(2M_g+1)\times 1}$ are calculated from the reference microphone signals $\boldsymbol{b} \in \mathbb{C}^{N_r \times 1}$. In matrix form, the global mode coefficients are represented as $\boldsymbol{\epsilon} = \boldsymbol{T}_e\boldsymbol{e}$ and $\boldsymbol{\beta} = \boldsymbol{T}_r\boldsymbol{b}$, where $\boldsymbol{T}_e$ and $\boldsymbol{T}_r$ are the transformation matrices.

2.3. Higher-order sources

In many sound field control techniques (e.g., sound field reproduction [26] and spatial ANC [9] techniques), the directivity pattern of sources is assumed to be omnidirectional. In [27], fixed-directivity sources were employed to reduce an undesirable reverberant field. Sound field control methods using the HOS array [14–20], which has a controllable directivity pattern, make it possible to achieve a more accurate reproduction of the desired sound field and suppression of the unwanted exterior sound field.

An ideal 2D higher-order source placed at $\boldsymbol{r}_{i_l} = (r_{i_l}, \phi_{i_l})$ in polar coordinate produces the sound field [14]

$$p_{i_l}(\boldsymbol{r}_o) = \sum_{m_l=-M_l}^{M_l} H_{m_l}^{(2)}(ka_{i_l,o})e^{-jm_l\theta_{i_l,o}}, \tag{3}$$

where $\theta_{i_l,o}$ is the angle from the field point $\boldsymbol{r}_o = (r_o, \phi_o)$ to the source vector $\boldsymbol{r}_{i_l}$ and $a_{i_l,o} = \|\boldsymbol{a}_{i_l,o}\|_2 = \|\boldsymbol{r}_o - \boldsymbol{r}_{i_l}\|_2$ (see Fig. 2). m_l is the order index of the HOS and is referred to as the local order in this paper. M_l is the maximum local order achievable from a particular loudspeaker configuration. Note that in practical implementation, the achievable maximum local order of the source depends on the time frequency and the configuration of the loudspeakers [15]. $H_m^{(2)}(\cdot)$ is the m^{th}-order Hankel function of the second kind.

When HOSs are located at $\boldsymbol{r}_1, \cdots \boldsymbol{r}_{N_l}$, the global mode coefficients of the sound field produced by them are derived using the cylindrical addition theorem [28] as

$$\begin{aligned} p(\boldsymbol{r}_o) &= \sum_{i_l, m_l} y_{m_l,i_l} H_{m_l}^{(2)}(ka_{i_l,o})e^{-jm_l\theta_{i_l,o}} \\ &= \sum_{i_l,m_l,m_g} y_{m_l,i_l} H_{m_g+m_l}^{(2)}(kr_l)J_{m_g}(kr_o)e^{-jm_g(\phi_o-\phi_{i_l})}, \end{aligned} \tag{4}$$

where y_{m_l,i_l} is the m_l^{th}-order complex amplitude of the i_l^{th} HOS, which is referred to as a local mode coefficient. From (1) and (4), we obtain the relationship between the global mode coefficients and the local mode coefficients as

$$\boldsymbol{\gamma} = \boldsymbol{g}[\cdots, \boldsymbol{H}_{m_l}\boldsymbol{F}^H, \cdots] \begin{bmatrix} \vdots \\ \boldsymbol{y}_{m_l} \\ \vdots \end{bmatrix} = \boldsymbol{gHy}, \tag{5}$$

$$\begin{aligned} \text{with } \boldsymbol{H}_{m_l} &= \mathrm{diag}\left(\frac{H_{-M_g+m_l}^{(2)}(kr_l)}{H_{-M_g}^{(2)}(kr_l)}, \cdots, \frac{H_{M_g+m_l}^{(2)}(kr_l)}{H_{M_g}^{(2)}(kr_l)}\right), \\ \boldsymbol{g} &= \mathrm{diag}\left(H_{-M_g}^{(2)}(kr_l), \cdots, H_{M_g}^{(2)}(kr_l)\right), \\ \boldsymbol{F} &\in \mathbb{C}^{N_l\times(2M_g+1)},\ (\boldsymbol{F})_{i_l,m_g} = e^{-jm_g\phi_{i_l}}, \\ m_l &= -M_l, \cdots, M_l, \end{aligned} \tag{6}$$

where $(\cdot)^H$ is the Hermitian transpose operator and $(\cdot)_{n,m}$ represents the $(n,m)^{\mathrm{th}}$ element of a matrix. $\boldsymbol{y}_{m_l} = [y_{m_l,1}, \cdots, y_{m_l,N_l}]^T \in \mathbb{C}^{N_l\times 1}$ is the HOS signals of a particular local mode. We define the concatenated matrix $\boldsymbol{H} \in \mathbb{C}^{(2M_g+1)\times(2M_l+1)N_l}$ and the concatenated vector $\boldsymbol{y} \in \mathbb{C}^{(2M_l+1)N_l\times 1}$ as (5).

3. PROPOSED ALGORITHMS IN MODE DOMAIN

In this section, we propose two types of adaptive ANC algorithm and compare them in Sec. 3.3. Both algorithms are based on the FxLMS algorithm [4]. To apply the FxLMS algorithm, an estimate of the secondary path, which is the transfer function between the secondary sources and the error sensors, is needed [4, 10]. In this case, it is an acoustical transfer function (ATF) from each local mode of the HOS to the error microphone array. We denote the actual ATF as $\boldsymbol{G} \in \mathbb{C}^{N_e\times(2M_l+1)N_l}$ and its estimate as $\hat{\boldsymbol{G}}$.

3.1. Local mode-domain adaptive algorithm

In this algorithm, the output signals of an HOS array are obtained directly as $\boldsymbol{y} = \boldsymbol{W}_l\boldsymbol{\beta}$ by linear filtering of the reference global mode coefficients $\boldsymbol{\beta}$, where $\boldsymbol{W}_l \in \mathbb{C}^{(2M_l+1)N_l\times(2M_g+1)}$ is the filter coefficient matrix. By denoting the global mode coefficients of the primary noise field as $\boldsymbol{\gamma} = [\gamma_{-M_g}, \cdots, \gamma_{M_g}]$, those of the residual noise field $\boldsymbol{\epsilon}$ are represented as

$$\boldsymbol{\epsilon} = \boldsymbol{\gamma} + \boldsymbol{T}_e\boldsymbol{G}\boldsymbol{W}_l\boldsymbol{\beta}. \tag{7}$$

The proposed adaptive algorithm minimizes the instantaneous squared error of the global mode coefficients as in [9], which is

$$J_g(\boldsymbol{\epsilon}(n)) = \boldsymbol{\epsilon}^H(n)\boldsymbol{\epsilon}(n), \tag{8}$$

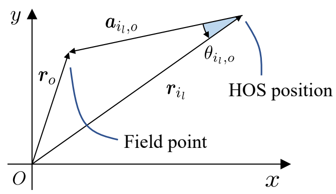

Fig. 2: Coordinate system of HOS.

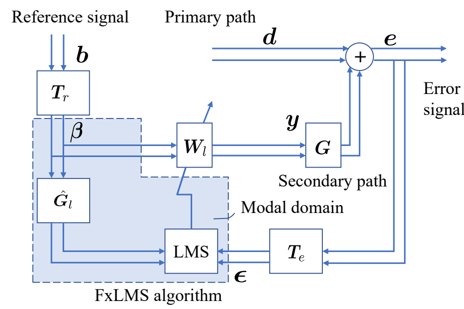

Fig. 3: Block diagram of **LM** algorithm.

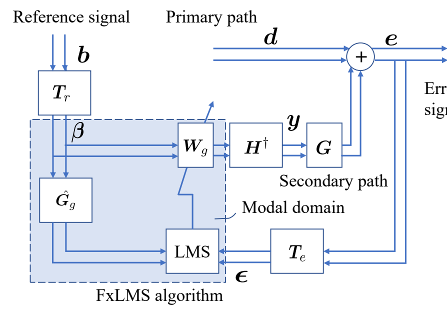

Fig. 4: Block diagram of **GM** algorithm.

where n represents the iteration index. Since the partial derivative of J_g with respect to $\overline{\boldsymbol{W}_l}$ ($\overline{\cdot}$ denotes the complex conjugate) is $\partial J_g/\partial\overline{\boldsymbol{W}_l} = (\boldsymbol{T}_e\boldsymbol{G}_l)^H\boldsymbol{\epsilon}(n)\boldsymbol{\beta}^H(n)$ [29, 30], we have the following update equation for the filter coefficients:

$$\boldsymbol{W}_l(n+1) = \boldsymbol{W}_l(n) - \mu\hat{\boldsymbol{G}_l}^H\boldsymbol{\epsilon}(n)\boldsymbol{\beta}^H(n), \tag{9}$$

where μ is the step size of the adaptation, $\boldsymbol{G}_l = \boldsymbol{T}_e\boldsymbol{G}$, and $\hat{\boldsymbol{G}}_l$ is an estimate of $\boldsymbol{G}_l$. A block diagram of this algorithm is shown in Fig. 3. As the output signals of the filter in this algorithm are the local mode coefficients, we denote the algorithm as **LM** in this paper.

3.2. Global mode-domain adaptive algorithm

In this algorithm, a filtering process and a filter update process are independently conducted in the global mode as in [9] to reduce the computational cost. Therefore, the filter output is the global mode coefficients and the filter coefficient matrix $\boldsymbol{W}_g \in \mathbb{C}^{(2M_g+1)\times(2M_g+1)}$ is the diagonal matrix. The signals of the HOS array are obtained as $\boldsymbol{y} = \boldsymbol{H}^\dagger\boldsymbol{W}_g\boldsymbol{\beta}$ by applying the pseudoinverse of $\boldsymbol{H}$ in (6) to the filter output $\boldsymbol{W}_g\boldsymbol{\beta}$, where $(\cdot)^\dagger$ represents the pseudoinverse of a matrix. As in Sec. 3.1, the global mode coefficients of the residual noise field are represented as

$$\boldsymbol{\epsilon} = \boldsymbol{\gamma} + \boldsymbol{T}_e\boldsymbol{G}\boldsymbol{H}^\dagger\boldsymbol{W}_g\boldsymbol{\beta}. \tag{10}$$

This algorithm also minimizes J_g in (8), and the partial derivative with respect to $\overline{\boldsymbol{W}_g}$ is derived similarly and is $\partial J_g/\partial\overline{\boldsymbol{W}_g} = (\boldsymbol{T}_e\boldsymbol{G}\boldsymbol{H}^\dagger)^H\boldsymbol{\epsilon}(n)\boldsymbol{\beta}^H(n)$. We here define an estimate of the secondary path in the mode domain as follows:

$$\hat{\boldsymbol{G}}_g = \mathrm{diag}\left((\boldsymbol{T}_e\hat{\boldsymbol{G}}\boldsymbol{H}^\dagger)_{-M_g,-M_g}, \cdots, (\boldsymbol{T}_e\hat{\boldsymbol{G}}\boldsymbol{H}^\dagger)_{M_g,M_g}\right). \tag{11}$$

Note that $\boldsymbol{T}_e\boldsymbol{G}\boldsymbol{H}^\dagger$ is equivalent to $\boldsymbol{g}$ in (6) when the sound field is assumed to be a free field and the HOSs have the ideal characteristics described in (3). When there are only 0^{th}-order sources, $\boldsymbol{T}_e\boldsymbol{G}\boldsymbol{H}^\dagger$ is approximated as a diagonal matrix even in a reverberant environment [9]. In Sec. 4, we show that it can also be approximated as a diagonal matrix when using the HOS array. We have the following filter update equation for this algorithm using $\hat{\boldsymbol{G}}_g$:

$$\boldsymbol{W}_g(n+1) = \boldsymbol{W}_g(n) - \mu\hat{\boldsymbol{G}_g}^H\left(\boldsymbol{\epsilon}(n)\circ\overline{\boldsymbol{\beta}(n)}\right), \tag{12}$$

where "$\circ$" denotes the Hadamard product. The Hadamard product for $\boldsymbol{\epsilon}(n)$ with $\overline{\boldsymbol{\beta}(n)}$ is calculated so that only the diagonal elements of $\boldsymbol{W}_g$ are updated.

In accordance with the **LM** algorithm, since the filter outputs are the global-mode coefficients, we denote this algorithm as **GM**. A block diagram of this algorithm is shown in Fig. 4.

Table 1: Comparison of computational cost

	Filtering	Filter update
LM	$\mathcal{O}((2M_l{+}1)N_l(2M_g{+}1))$	$\mathcal{O}((2M_l{+}1)N_l(2M_g{+}1))$
GM	$\mathcal{O}((2M_l{+}1)N_l(2M_g{+}1))$	$\mathcal{O}(2M_g{+}1)$
MIMO	$\mathcal{O}((2M_l{+}1)N_lN_r)$	$\mathcal{O}((2M_l{+}1)N_l(N_r{+}N_e))$

3.3. Comparison between proposed algorithms

3.3.1. Computational cost

Table 1 shows the computational cost of **LM**, **GM**, and the multipoint algorithm (**MIMO**) [7]. **GM** has a significantly lower computational cost for the filter update process than **LM** and **MIMO**. In the filtering process of **GM**, there are no significant differences in costs between **LM** and **GM** in this process. This is because the cost of applying $\boldsymbol{H}^\dagger$ is $\mathcal{O}\left((2M_l+1)N_l(2M_g+1)\right)$, although the cost of applying the filter $\boldsymbol{W}_g$ to the reference signals $\boldsymbol{\beta}$ is low.

3.3.2. HOS array configuration

Although in Sec. 2.1 a circular equiangular HOS array is assumed, **LM** does not necessarily require this configuration. It is advantageous in practical cases because the adaptation compensates for the degradation in the performance due to the positional deviation of elements in the array. **GM** is sensitive to the deviation because r_l is assumed to be a constant value in (6) and $\boldsymbol{T}_e\hat{\boldsymbol{G}}\boldsymbol{H}^\dagger$ can no longer be approximated by a diagonal matrix when there is deviation.

4. SIMULATIONS

We conducted numerical simulations of spatial ANC to compare the proposed algorithms (**GM**, **LM**) with the conventional multipoint algorithm (**MIMO**) [7], which has the FxLMS structure and calculates the error in the spatial domain as $J(\boldsymbol{e}) = \boldsymbol{e}^H\boldsymbol{e}$. A 2D sound field was assumed, and three circular equiangular transducer arrays were located as shown in Fig. 1. When we assume a circular array in a 3D sound field, which can be implemented more practically, the *secondary source type mismatch* [31] should be considered. The radii of the reference, the HOS, and the error arrays were 1.60, 1.35, and 1.10 m and the numbers of array elements were 48, 12, and 48, respectively. The radius of the target area r_{target} was set to 1.00 m. A reverberant room environment was simulated using the generalized image-source method [32]. The image order was set to 3. The room size was 6 m $\times$ 8 m and all the reflection coefficients of the walls were set to 0.6. The room had the reverberation time RT_{60} of 230 ms.

A single omnidirectional noise source was located at (2.0, 2.4) m. The noise source signal was a single-frequency sinusoidal wave whose frequency was in the range of 100–800 Hz. Its complex amplitude was generated from a complex Gaussian distribution.

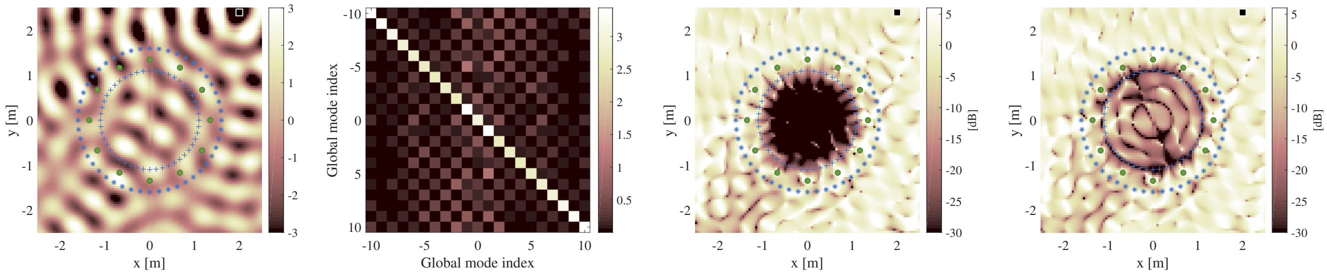

(a) (b) (c) (d)

Fig. 5: (a) Primary noise field in reverberant environment. (b) Secondary path of **GM** ($\boldsymbol{T}_e\boldsymbol{G}\boldsymbol{H}^\dagger$). (c)(d) Noise level in dB after 500 iterations when applying (c) **LM** and (d) **MIMO**.

The maximum local order of the HOS was set to 0, 1, and 2 when the noise frequency was in the ranges of 100–200, 200–500, and 500–800 Hz, respectively. When applying each algorithm, the filter update equation was modified by its normalized version [4], in which the update term was divided by the power of the filtered reference signals. The step size was set to 0.1.

Fig. 5a shows the real part of the primary noise field in the simulated reverberant environment. The marks "$*$", "$\circ$", "$+$", and "■" represent the reference microphones, the HOSs, the error microphones, and the noise source, respectively. The frequency of the noise signal was 500 Hz. The maximum global order was set to 10 because $\lceil kr_{\mathrm{target}} \rceil = 10$ [23]. Measurement noise was added to the signals of the reference and error microphone array so that the source-to-noise ratio (SNR) was 40 dB. The magnitude of the secondary path of **GM** in this setup, which is defined as $\boldsymbol{T}_e\boldsymbol{G}\boldsymbol{H}^\dagger$, is shown in Fig. 5b. We observed that the matrix has dominant diagonal components, which can be diagonalized to $\boldsymbol{g}$ in (6).

Figs. 5c and 5d show noise levels in dB after 500 iterations when applying **LM** and **MIMO**, respectively. The noise level at a field point $\boldsymbol{r}$ was calculated as $10\log_{10}(|p_{\mathrm{res}}(\boldsymbol{r})|^2/|p_{\mathrm{pri}}(\boldsymbol{r})|^2)$, where $p_{\mathrm{res}}(\cdot)$ and $p_{\mathrm{pri}}(\cdot)$ represent the sound pressures of the residual and primary noise fields, respectively. The noise levels in the target area when applying **GM**, **LM**, and **MIMO** were –22.54, –26.95, and –14.16 dB, respectively. They were calculated as $10\log_{10}(\sum_i |p_{\mathrm{res}}(\boldsymbol{r}_i)|^2/\sum_i |p_{\mathrm{pri}}(\boldsymbol{r}_i)|^2)$, where $\boldsymbol{r}_i$ represents a grid point in the target area. The interval of the grid points was set to 0.05 m. Although **MIMO** reduced the noise level at only the control points, **LM** and **GM** attenuated the noise over the entire target area.

Fig. 6 shows the relationship between the number of iterations and the averaged noise level of the error microphone signals $\boldsymbol{e}$ (Spatial), the residual global mode coefficients $\boldsymbol{\epsilon}$ (Modal), and the residual noise in the target area (Target). The simulation setup was the same as that in the previous paragraph. **GM** and **LM** achieved rapid convergence because they adopt mode-domain signal processing.

Fig. 7 shows the relationship between the frequency of the noise source and the amount of noise reduction when there was a deviation in the positions of the elements in the HOS array. The SNR of the measurement noise was 40 dB. The number of iterations was 500. "15 cm" represents the maximum positional deviation of the array elements. The lengths of the deviations were randomly drawn from the uniform distribution. "0 cm" means that there was no deviation. When deviation occured, the performance of **GM** significantly deteriorated above 500 Hz because **GM** assumes a circular equiangular transducer array. In contrast, **LM** had robustness against the deviation and a high performance, especially above 500 Hz.

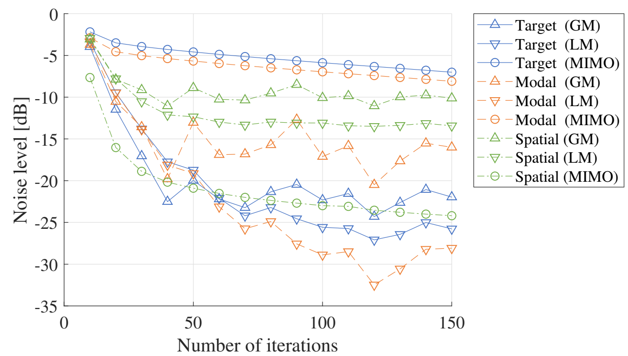

Fig. 6: Comparison of convergence ratio for each algorithm. Each plot shows average noise level over latest 10 iterations.

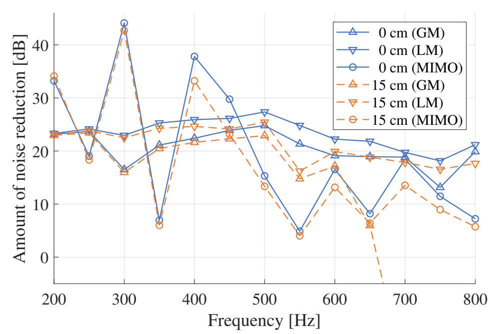

Fig. 7: Relationship between frequency and amount of noise reduction when positional deviation of HOSs occurs.

5. CONCLUSION

To overcome the practical issues arising from large-scale spatial ANC, such as a high computational cost and the space occupied by loudspeakers, we devised two different mode-domain adaptive algorithms using HOSs, which provide a trade-off between efficiency and error robustness against loudspeaker placements. Numerical simulations in a reverberant environment showed that the proposed algorithms controlled the entire target area and had a high convergence speed compared with the conventional multipoint algorithm. The experiment also revealed that **GM** requires a lower computational cost than **LM**, whereas **LM** is more robust against positional deviation.

6. REFERENCES

[1] S. M. Kuo, S. Mitra, and W. S. Gan, "Active noise control system for headphone applications," *IEEE Trans. Control Syst. Technol.*, vol. 14, no. 2, pp. 331–335, 2006.

[2] S. J. Elliott and P. A. Nelson, "Active noise control," *IEEE Signal Process. Mag.*, vol. 10, no. 4, pp. 12–35, 1993.

[3] J. C. Burgess, "Active adaptive sound control in a duct: A computer simulation," *J. Acoust. Soc. Am.*, vol. 70, no. 3, pp. 715–726, 1981.

[4] S. J. Elliott, *Signal processing for active control*, Elsevier, 2000.

[5] C. Hansen, S. Snyder, X. Qiu, L. Brooks, and D. Moreau, *Active control of noise and vibration*, CRC Press, 2012.

[6] S. Narayan, A. Peterson, and M. Narasimha, "Transform domain LMS algorithm," *IEEE Trans. Acoust. Speech Signal Process.*, vol. 31, no. 3, pp. 609–615, 1983.

[7] S. M. Kuo and D. Morgan, *Active noise control systems: algorithms and DSP implementations*, John Wiley & Sons, Inc., 1995.

[8] E. G. Williams, *Fourier acoustics: sound radiation and nearfield acoustical holography*, Elsevier, 1999.

[9] J. Zhang, T. D. Abhayapala, W. Zhang, P. N. Samarasinghe, and S. Jiang, "Active noise control over space: A wave domain approach," *IEEE/ACM Trans. Audio Speech Lang. Process.*, vol. 26, no. 4, pp. 774–786, 2018.

[10] W. Zhang, C. Hofmann, M. Burger, T. D. Abhayapala, and W. Kellermann, "Spatial noise-field control with online secondary path modeling: A wave-domain approach," *IEEE/ACM Trans. Audio Speech Lang. Process.*, vol. 26, no. 12, pp. 2355–2370, Aug. 2018.

[11] Y. Maeno, Y. Mitsufuji, and T. D. Abhayapala, "Mode domain spatial active noise control using sparse signal representation," in *Proc. IEEE Int. Conf. Acoust., Speech, Signal Process. (ICASSP)*, 2018, pp. 211–215.

[12] Y. Maeno, Y. Mitsufuji, P. N. Samarasinghe, and T. D. Abhayapala, "Mode-domain spatial active noise control using multiple circular arrays," in *Proc. Int. Workshop Acoust. Signal Enhancement (IWAENC)*, Sep. 2018, pp. 441–445.

[13] H. Ito, S. Koyama, N. Ueno, and H. Saruwatari, "Feedforward spatial active noise control based on kernel interpolation of sound field," in *Proc. IEEE Int. Conf. Acoust., Speech, Signal Process. (ICASSP)*. IEEE, 2019, (to appear).

[14] M. A. Poletti and T. D. Abhayapala, "Spatial sound reproduction systems using higher order loudspeakers," in *Proc. IEEE Int. Conf. Acoust., Speech, Signal Process. (ICASSP)*. IEEE, 2011, pp. 57–60.

[15] M. A. Poletti and T. Betlehem, "Design of a prototype variable directivity loudspeaker for improved surround sound reproduction in rooms," in *Audio Engineering Society Conference: 52nd International Conference: Sound Field Control-Engineering and Perception*. Audio Engineering Society, 2013.

[16] P. N. Samarasinghe, M. A. Poletti, S. M. A. Salehin, T. D. Abhayapala, and F. M. Fazi, "3D soundfield reproduction using higher order loudspeakers," in *Proc. IEEE Int. Conf. Acoust., Speech, Signal Process. (ICASSP)*. IEEE, 2013, pp. 306–310.

[17] T. Betlehem and M. A. Poletti, "Two dimensional sound field reproduction using higher order sources to exploit room reflections," *J. Acoust. Soc. Am.*, vol. 135, no. 4, pp. 1820–1833, 2014.

[18] K. Wakayama and H. Takada, "Spatial multi-zone sound field reproduction using higher-order loudspeakers in reverberant rooms," in *Audio Engineering Society Convention 140*. Audio Engineering Society, 2016.

[19] M. Jia, W. Wang, and Z. Yang, "2.5 D sound field reproduction using higher order loudspeakers," *cybernetics and information technologies*, vol. 15, no. 6, pp. 5–15, 2015.

[20] F. Zotter, H. Pomberger, and A. Schmeder, "Efficient directivity pattern control for spherical loudspeaker arrays," *J. Acoust. Soc. Am.*, vol. 123, no. 5, pp. 3643, 2008.

[21] S. C. Douglas, "Fast implementations of the filtered-X LMS and LMS algorithms for multichannel active noise control," *IEEE Trans. Speech Audio Process.*, vol. 7, no. 4, pp. 454–465, 1999.

[22] M. A. Poletti, "A unified theory of horizontal holographic sound systems," *J. Audio Eng. Soc.*, vol. 48, no. 12, pp. 1155–1182, 2000.

[23] D. B. Ward and T. D. Abhayapala, "Reproduction of a plane-wave sound field using an array of loudspeakers," *IEEE Trans. Speech Audio Process.*, vol. 9, no. 6, pp. 697–707, 2001.

[24] P. Grandjean, P. A. Gauthier, and A. Berry, "Size of the accurate-reproduction area as function of directional metrics in spherical harmonic domain," in *Audio Engineering Society Conference: 2018 AES International Conference on Spatial Reproduction-Aesthetics and Science*. Audio Engineering Society, 2018.

[25] J. Zhang, W. Zhang, and T. D. Abhayapala, "Noise cancellation over spatial regions using adaptive wave domain processing," in *Proc. IEEE Int. Workshop Appl. Signal Process. Audio Acoust. (WASPAA)*. IEEE, 2015, pp. 1–5.

[26] M. A. Poletti, "Three-dimensional surround sound systems based on spherical harmonics," *J. Audio Eng. Soc.*, vol. 53, no. 11, pp. 1004–1025, 2005.

[27] M. A. Poletti, F. M. Fazi, and P. A. Nelson, "Sound-field reproduction systems using fixed-directivity loudspeakers," *J. Acoust. Soc. Am.*, vol. 127, no. 6, pp. 3590–3601, 2010.

[28] P. A. Martin, *Multiple scattering: interaction of time-harmonic waves with N obstacles*, Number 107. Cambridge University Press, 2006.

[29] K. B. Petersen, M. S. Pedersen, et al., "The matrix cookbook," *Technical University of Denmark*, vol. 7, no. 15, pp. 510, 2008.

[30] D. H. Brandwood, "A complex gradient operator and its application in adaptive array theory," in *IEE Proceedings H-Microwaves, Optics and Antennas*. IET, 1983, vol. 130, pp. 11–16.

[31] S. Spors, R. Rabenstein, and J. Ahrens, "The theory of wave field synthesis revisited," in *124th AES Convention*. Audio Engineering Society, 2008, pp. 17–20.

[32] P. N. Samarasinghe, T. D. Abhayapala, Y. Lu, H. Chen, and G. Dickins, "Spherical harmonics based generalized image source method for simulating room acoustics," *J. Acoust. Soc. Am.*, vol. 144, no. 3, pp. 1381–1391, 2018.